Analyst

Accepted Manuscript

ROYAL SOCIETY OF CHEMISTRY

www.rsc.org/analyst

Cite this: DOI: 10.1039/c0xx00000x

www.rsc.org/xxxxxx

ARTICLE TYPE

Electrochemical protein-based biosensor for detection of tau protein, a neurodegenerative disease biomarker

Jose O. Esteves-Villanueva, Hanna Trzeciakiewicz and Sanela Martic*

Received (in XXX, XXX) Xth XXXXXXXXX 20XX, Accepted Xth XXXXXXXXX 20XX

DOI: 10.1039/b000000x

The protein-based electrochemical biosensor was developed for detection of the tau protein aimed towards electrochemically sensing misfolding proteins. The electrochemical assay monitors tau-tau binding and misfolding during the early stage of tau oligomerization. Electrochemical impedance spectroscopy was used to detect binding event between solution tau protein and the immobilized tau protein (tau-Au), acting as a recognition element. The charge transfer resistance (R_{ct}) of tau-Au was 2.9 ± 0.6 kΩ. Subsequent tau binding to tau-Au decreased the R_{ct} to 0.3 ± 0.1 kΩ (90 ± 3 % decrease) upon formation of tau-tau-Au interface. A linear relationship between R_{ct} and solution tau concentration was observed from 0.2 to 1.0 µM. The R_{ct} decrease was attributed to an enhanced charge permeability of tau-tau-Au surface to a redox probe $[Fe(CN)_6]^{3-/4-}$. The electrochemical and surface characterization data suggested conformational and electrostatic changes induced by tau-tau binding. The protein-based electrochemical platform was highly selective for tau protein over bovine serum albumin and allowed for a rapid sample analysis. The protein-based interface was selective for a non-phosphorylated tau441 isoform over the paired-helical filaments of tau, which were composed of phosphorylated and truncated tau isoforms. The electrochemical approach may find application in screening of the onset of neurodegeneration and aggregation inhibitors.

1. Introduction

The tau protein stabilizes microtubules in neuronal cells, but when hyperphosphorylated tau dissociates from microtubules and forms the neurofibrillary tangles (NFTs) and paired helical filaments (PHFs), which alongside amyloid-β plaques, are linked to neurodegeneration and Alzheimer's Disease.[1-4] Tau's tendency to self-associate is one of the triggers of its malfunction. Tau pathology is associated with the existence of insoluble filaments of tau, but recent findings identified soluble tau oligomers as additional toxic species.[5-8] The pathological tau is composed of phosphorylated tau protein, but nonphosphorylated tau protein may also aggregate. The mechanism of tau aggregation is still elusive. The morphological studies of the insoluble tau aggregates have been well documented, but the early stage of tau aggregation is largely unexplored. Aggregated tau is typically studied at the later stage (dominated by insoluble aggregates) by optical spectroscopy (Thioflavin T fluorescence and circular dichroism) and microscopy (transmission electron microscopy) which precludes discoveries of mechanism of tau aggregation and its potential inhibition.[9-11] The solution studies of early stage tau aggregation are challenging due to unfolded and disordered tau structure.[12-13] The onset of tau misfolding and conformational changes during early aggregation remains unidentified. Subsequently, the drug development targeting the prevention of early tau aggregation is a challenge.

The alternative analytical methods are needed for identification of new aggregation pathways and detection of tau oligomers at the early stage of tau aggregation towards early detection of neurodegeneration. Electrochemical impedance spectroscopy (EIS) is sensitive to protein conformational change and protein binding, requires small sample volume, and is easily extended to a bioassay platform for screening of biomarkers and inhibitors.[14-15] Importantly, the EIS experiments are non-invasive, and do not perturb protein conformation during measurement thus leaving the protein intact. EIS has been widely used for detection of protein-protein and protein-DNA interactions as well as for characterization of self-assembled monolayers and adsorption of proteins on surfaces.[16-24] The adsorption of protein modulates the impedance by hindering the current flow from solution redox probe across the electrode/electrolyte interface. In turn, the decreased electron transfer rates were observed between the electrode surface and the electrolyte for protein films composed of dehydrogenase, BSA, lysozyme, etc.[16-24]

The electrochemical investigations of the tau protein are scarce. The enzyme-catalyzed phosphorylations of tau have been detected by cyclic voltammetry (CV) in a labelled approach using ferrocene.[25-26] However, the tau-tau interactions in the early stages of aggregation have not been detected previously by electrochemical means. Up to our knowledge, there have been no previous reports on electrochemical detection of tau-tau protein

binding and conformational change. Here, the label-free electrochemical methods, EIS and CV, were used to detect and quantify the solution tau protein binding to the biosensing interface based on the immobilized tau protein on Au surface (tau-Au). The tau-tau binding on tau-Au interface was used as a model system towards development of the electrochemical assay for detection of early onset of tau misfolding. A largely soluble and disordered microtubule-associated protein tau (441 amino acids, 45.9 kDa) was chosen for this study. The binding of tau to tau-Au recognition element modulated the charge transfer resistance. Specifically, the factors such as tau concentration, temperature, solution pH, and ionic strength on tau-tau binding and the charge transfer resistance were tested. This study provides the first electrochemical evidence of tau-tau binding and the impact of electrostatic interactions and conformational changes in the early stage of tau misfolding.

2. Experimental

2.1 Chemicals and reagents

All proteins were used as received. The bovine serum albumin (BSA) was obtained from Amresco (OH, USA). Tau441 protein was purchased from rPeptides (GA, USA). The stock solution of phosphate buffer, pH 6.8, was prepared using 10 mM sodium phosphate monobasic, anhydrous obtained from Fisher Scientific (NJ, USA), and sodium phosphate dibasic, anhydrous from J.T. Baker (NJ, USA). The pH was adjusted with sodium hydroxide obtained from Fisher Scientific (NJ, USA). The 2-(N-morpholino)ethanesulfonic acid (MES), sodium chloride and ethylene diaminetetra acetic acid (EDTA) were purchased from Fisher Scientific (NJ, USA). The ethanolamine, hexanethiol, potassium ferricyanide(III) ($K_3[Fe(CN)_6]$), potassium ferrocyanide(II) ($K_4[Fe(CN)_6]$), hexaaammineruthenium(II) chloride ($Ru(NH_3)_6Cl_2$) and hexaaammineruthenium(III) chloride ($Ru(NH_3)_6Cl_3$) were purchased from Sigma-Aldrich (MO, USA). PHF sample precipitated with trichloroacetic acid isolated from Alzheimer's Disease mouse brain homogenate was a generous gift from Dr. Einar M. Sigurdsson (New York University School of Medicine, NY, USA).[27]

2.2 Electrochemical measurements

Electrochemical experiments were carried out using a CHI660D Potentiostat from CHInstruments Inc. (TX, USA). The gold disk electrodes (0.0314 cm^2 surface area) were purchased from CHInstruments Inc. (TX, USA). A conventional three electrode system, consisting of gold electrode as a working electrode, a platinum wire as an auxiliary electrode and Ag/AgCl/1.0M KCl as a reference electrode was used for all experiments. All electrochemical measurements were performed in 10 mM $[Fe(CN)_6]^{3-/4-}$ and 10 mM phosphate buffer, pH 6.8. CV was performed at a scan rate of 0.1 V s^{-1} and in the potential range between -0.4 to 0.7 V, unless otherwise specified. The electrode potential was measured vs. Ag/AgCl/1.0M KCl reference electrode. EIS was carried out starting at an open circuit potential (OCP), a frequency range between 1 Hz to 100 KHz, and applied amplitude of 5 mV. Experimental EIS data were fitted with an equivalent circuit using ZSimp Win 3.22 (Princeton Applied Research). Fitted and experimental data were presented in the form of Nyquist or Bode plots. The charge transfer resistance, R_{ct}, was determined by fitting the impedance data to the appropriate equivalent circuit and was expressed in Ω or kΩ. All experiments were performed in triplicates and the corresponding error bars represent the standard deviations.

2.3 Ellipsometry

Single-wavelength ellipsometry was performed on a LSE Stokes Ellipsometer. The light source was a HeNe measuring laser with 632.8 nm wavelength, and at 70 ° angle of incidence. Au (sputtering) substrate had the characteristic refractive index, n_s, and extinction coefficient, k_s, values of 0.25 and 3.24, respectively. Each sample was compared to the bare Au substrate. Thickness was calculated by the NI-DAQmx Software. Each sample was tested in duplicates.

2.4 Contact angle measurements

Contact angle (θ) was measured using the method based on the diameter of a 10 µL sessile drop of 10 mM phosphate buffer at pH of 6.8 to distinguish surface wettability of tau-Au and tau-tau-Au. The contact angle of bare Au substrate was determined to be 72 °. Each sample was tested in duplicates.

2.5 Preparation of tau-Au surface

The Au electrodes were cleaned as follow: (1) etching in piranha solution for 5 min (3:1 v/v % H_2SO_4:H_2O_2), (2) hand polishing in alumina (1 µm, 0.3 µm and 0.05 µm) for 1 min each, and (3) sonicating in deionized water for 10 min. Electrochemical cleaning was performed by CV in 0.5 M KOH solution at 0.5 V/s in the -2 - 0 V potential range, followed by cyclic voltammetry in 0.5 M H_2SO_4 at 0.5 V/s in the 0 - 1.5 V potential range. The clean Au electrodes were rinsed with deionized water, dried under N_2 flow, and then incubated in a 2 mM solution of Lipoic acid N-hydroxysuccinimide ester (Lip-NHS) in ethanol for 3 d at 5 °C. The Lip-NHS was synthesized in house following the published protocol.[28] After, the Lip-NHS-Au electrodes were rinsed with ethanol. For tau protein immobilization, Lip-NHS-Au electrodes were incubated with 0.2 µM tau solution (50 mM MES, pH 6.8, 100 mM NaCl, and 0.5 mM EDTA) for 24 h at 5 °C. The tau-Au electrodes then were rinsed with 10 mM phosphate buffer, pH of 6.8, and immersed in 100 mM ethanolamine solution for 1 h at room temperature. Next, incubation in 10 mM hexanethiol solution was carried out for 20 min at room temperature. Subsequently, the electrodes were rinsed with 10 mM phosphate buffer solution, pH 6.8 prior to electrochemical measurements.

2.6 Protein binding experiments

Tau-Au was incubated in 5 µL of various solutions for 2 h at 37 °C, unless otherwise mentioned. The tau concentration experiments were carried out at 0.1, 0.2, 0.4, 0.8, 1.0, 2.0, 4.0, 5.0 and 10 µM (50 mM MES, pH 6.8, 100 mM NaCl, and 0.5 mM EDTA). Time-dependent studies were performed by incubating tau-Au with 5 µM tau solution at different time intervals: 1, 2, 30, 60, 90 and 120 min. The pH-dependent experiments were performed at pH 6.8 or 8.5. The tau-free surface was prepared as

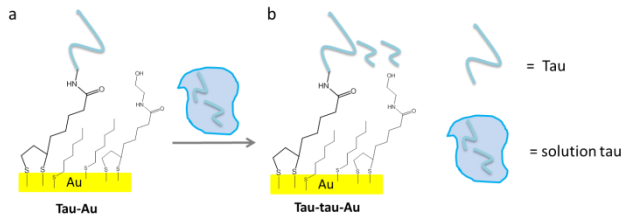

Scheme 1 Illustration of the tau-based biosensor (a) for detection of tau-tau binding to obtain tau-tau-Au surface (b).

described above without the tau immobilization step. The BSA studies were carried out at 5 µM BSA concentration. The buffer-tau-Au was carried out by exposing tau-Au to a solution free of tau protein, solely the incubating buffer.

2.7 Sample preparation for surface characterization

The samples for surface characterization were prepared using Au sputtered silicon wafers (Nanofabrication Facility, Western University, Canada). The silicon wafer was coated with 6 nm Ti followed by 140 nm Au. The Au wafer was sliced into 1 × 1 cm substrates. The Au substrates were cleaned by etching with piranha solution for 5 min and rinsing with copious amount of DI water. Next, the substrates were rinsed with ethanol and dried with N_2. For tau-Au preparation the stepwise modification steps were identical to those described in subsection 2.3. The tau binding was carried out at 5 µM tau, pH 6.8, for 2 h at 37 °C. Finally, substrates were rinsed with 10 mM phosphate buffer, pH 6.8 and measured by ellipsometry and contact angle measurements.

3. Results and discussion

The electrochemical approach for detection of solution tau protein binding to the immobilized tau-Au interface is depicted in Scheme 1. The tau-Au interface (a) was exposed to the protein solution under variety of conditions forming tau-tau-Au interface (b). The modulation in the charge transfer resistance was monitored as a function of protein concentration, solution pH, ionic strength and incubation time and temperature.

3.1 Preparation and electrochemical characterization of tau-Au surface

To prepare tau-Au surface (a), the tau441 protein was immobilized on Au electrode using amide coupling as previously described for tau410 protein.[25-26] Briefly, the tau was immobilized *via* bifunctional disulfide, lipoic acid *N*-hydroxysuccinimide ester (Lip-NHS), tethered to the Au surface. Next, the unreacted NHS sites were blocked with ethanolamine, and then the exposed Au surfaces were backfilled with hexanethiol diluent to prevent nonspecific adsorption of the protein. At this step tau-Au interface was fabricated, illustrated in Scheme 1a, and was exposed next to the solution containing tau.

The stepwise fabrication of tau-Au surface was characterized by CV as in Fig. 1A in the presence of the redox couple $[Fe(CN)_6]^{3-/4-}$. The bare-Au (a) electrode exhibited the reversible oxidation/reduction peaks at high current density (Fig. 1A).

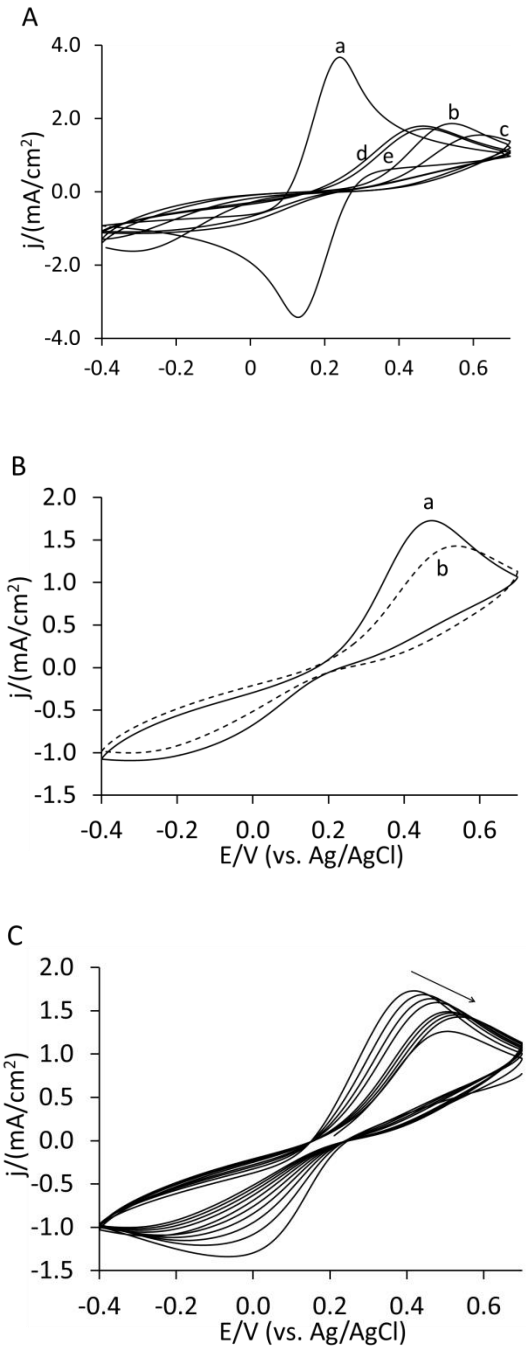

Fig. 1 (A) Cyclic voltammograms of bare-Au (a), Lip-NHS-Au (b), tau-Au (c), ethanolamine-tau-Au (d), and hexanethiol-ethanolamine-tau-Au (e). (B) Cyclic voltammograms of tau-Au (a) and tau-tau-Au (b). (C) Cyclic voltammograms of tau-tau-Au as a function of a number of scans (10 mM $[Fe(CN)_6]^{3-/4-}$,10 mM phosphate buffer, pH 6.8, arrows indicate cycling direction and increasing number of scans, 100 mV s^{-1} scan rate).

During stepwise modifications, the current decreased and the potential peak separation increased. The immobilization of the Lip-NHS (b) and subsequent tau attachment (c) decreased the current density and increased the potential peak separation. Subsequent blocking with ethanolamine (d) and backfilling with hexanethiol (e) produced the final tau-Au interface. The final tau-Au interface was characterized prior to protein binding studies. The low current density and large peak separation observed in CV of tau-Au (a) in Fig. 1B indicated the successful surface coverage and tau-Au fabrication. The cyclic voltammogram vs. scan rate measurements of tau-Au surface revealed a linear relationship of current, I_p, with the square root of scan rate, $v^{1/2}$, indicating the diffusion-controlled electrochemical reaction rate for the redox pair (Fig. S2-S3, ESI†). Both anodic and cathodic peak currents were proportional to the scan rate from 5 to 900 mV s^{-1}.

The stepwise fabrication of tau-Au surface was also monitored by EIS. The bare-Au (a) electrode was characterized by diffusion-controlled process (Fig. 2A). The immobilization of lip-NHS (b) followed by incubation in tau (c) produced a large resistance. Next, the blocking with ethanolamine (d) and backfilling with hexanethiol (e) resulted in a decrease in resistance which may be due to removal of non-specifically adsorbed tau protein on the surface. The final tau-Au surface was characterized by a charge transfer resistance of 2.8 ± 0.6 kΩ.

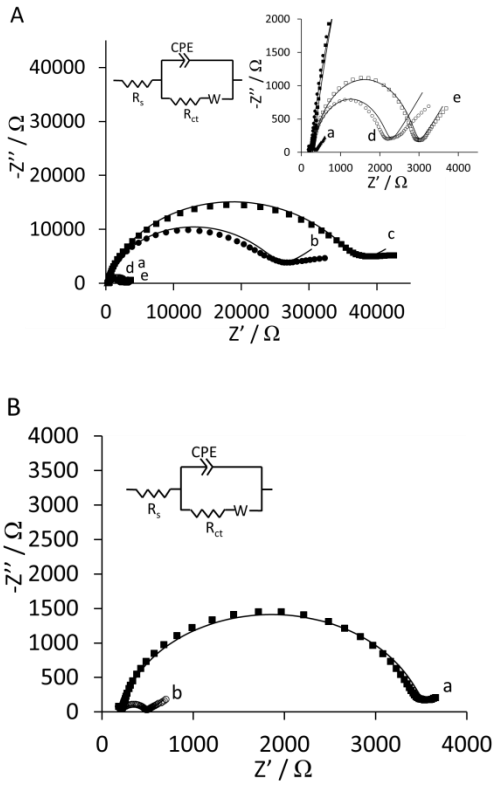

Fig. 2 (A) Nyquist plots of bare-Au (a), Lip-NHS-Au (b), tau-Au (c), ethanolamine-tau-Au (d), and hexanethiol-ethanolamine-tau-Au (e). (B) Nyquist plots of tau-Au (a) and tau-tau-Au (b) interface (inset equivalent circuit used to fit the experimental impedance data, 10 mM phosphate buffer, pH 6.8, 10 mM $[Fe(CN)_6]^{3-/4-}$).

The real and imaginary parts of the impedance were monitored for tau-Au (a) and plotted in Fig. 2B. The real and imaginary parts of the impedance are calculated from eqn (1):

$$Z^*(\omega) = Z'(\omega) + jZ''(\omega) \quad (1)$$

where $Z'(\omega)$ is the real impedance, $Z''(\omega)$ is the imaginary impedance and equals $-1\ \omega C^{-1}$, ω is the angular frequency which equals $2\pi f$ (f/Hz is the ac frequency). The impedance data were fitted to the equivalent circuit, illustrated in Fig. 2 (inset) comprised of the electrolyte solution, R_s, tau protein electrode interface (constant phase element, *CPE*, and charge transfer resistance, R_{ct}) and Warburg constant, W.[29-30] R_s included contribution of the connections to the electrodes. R_{ct} is the charge transfer resistance and represents the impedance component through which the Faradaic current flows. W is the infinite Warburg impedance or resistance to mass transfer. The non-Faradaic current passes through the *CPE*, which comprises the double-layer capacitance; often the non-Faradaic current has been ascribed to the surface roughness, topological imperfections and contamination. The *CPE* is defined in terms of parameter Q and the exponent n as in eqn (2):

$$Z_{CPE} = 1/(Q(j\omega)^n) \quad (2)$$

wherein $Q/n\Omega^{-1}s^n$ is parameter used in the non-linear least square fitting routine. The *CPE* acts as a pure capacitor when n equals 1. Table 1 summarizes the values of the circuit elements obtained by fitting the experimental data for tau-Au surface. The tau-Au was characterized by R_{ct} of 2.91 ± 0.61 kΩ and n of 0.89 ± 0.01.

3.2 Electrochemical detection of tau protein

The solution tau binding to tau-Au surface was monitored by exposing tau-Au interface to the tau solution as illustrated in Scheme 1. The protein solution contained 5 µM tau, 50 mM MES, pH 6.8, 100 mM NaCl, and 0.5 mM EDTA. All binding studies were carried out at pH 6.8, 37˚C for 2 h, unless otherwise mentioned. The pH 6.8 is the biologically relevant pH for tau protein and favourable for tau aggregation.[31]

Table 1 Impedance parameters of tau-Au and tau-tau-Au surfaces fitted to the equivalent circuit.

	R_s[a] (kΩ)	Q[a] (µΩ^{-1}·s^n)	n[b]	R_{ct}[a] (kΩ)	W[c] (mΩ^{-1}·s$^{0.5}$)
Tau-Au	0.26 ± 0.04	0.58 ± 0.33	0.89 ± 0.01	2.91 ± 0.61	1.0 ± 0.3
Tau-tau-Au	0.08 ± 0.02	16.4 ± 7.31	0.39 ± 0.07	0.36 ± 0.08	1.4 ± 0.1

[a]R_s, Q, and R_{ct} are solution resistance, constant phase element and charge transfer resistance, respectively. [b]n is exponent. [c]W is Warburg resistance. The equivalent circuit used is given in Fig. 2 inset.

Following the binding studies, the electrodes were rinsed and measured by CV and EIS in the presence of 10 mM $[Fe(CN)_6]^{3-/4-}$ in 10 mM phosphate buffer, pH 6.8. Fig. 1B shows CV of tau-Au (a) prior to and following the binding of solution tau (b). The relatively similar potential separation between the cathodic and anodic waves and the low peak currents were maintained for tau-Au (a) and tau-tau-Au (b). However, tau-tau-Au film (b) appears to be more blocked. This was further supported by the continuous CV experiment as a function of the number of scans for tau-tau-Au (Fig. 1C). The cathodic and anodic currents decreased and potential peak separation increased with continuous scanning. The permeability of the tau-tau-Au film toward $[Fe(CN)_6]^{3-/4-}$ was reduced upon increased CV scanning. The potential shift and the decrease in the current density may imply that there is a structural rearrangement which induced the release of ions and uptake of solvent.[32] In addition, the diffusion of $[Fe(CN)_6]^{3-/4-}$ to the electrode surface was reduced, due to film rearrangement and formation of an insulating layer, resulting in the larger peak potential separation and the decrease in peak current.[33] With cycling, the shape of CV of tau-tau-Au changed suggesting tau binding to tau-Au surface and the film reorientation upon binding to produce a more blocked film (Fig. 1C). No loss of tau film in tau-tau-Au was observed since even after twenty cycles the CVs were stable and did not change. Tau-Au or tau-tau-Au film decomposition and loss from the surface were unlikely, because CV desorption studies in 0.5 M KOH showed similar surface coverage, Γ, for tau-Au ($2.9 \pm 0.3 \times 10^{-10}$ mol cm^{-2}) and tau-tau-Au ($2.5 \pm 0.3 \times 10^{-10}$ mol cm^{-2}) (Fig. S5, ESI†). The surface coverage was estimated by integrating the current of the cathodic peak, determining the average charge, Q, and using Faraday's law in eqn (3):

$$\Gamma = Q / nFA \quad (3)$$

Where, n is number of electrons transferred (n = 1), F is the Faraday constant (F = 96485 C mol^{-1}), and A is the geometric area of the electrode (0.0314 cm^2).

To further characterize tau-tau binding, the binding of solution tau to tau-Au interface was monitored by EIS. The impedance spectrum of tau-Au (a) in Fig. 2B exhibited the large depressed semi-circle, the small linear portion and R_{ct} value of 2.91 ± 0.61 kΩ. The electron transfer from the redox probe to Au electrode was largely charge-transfer limited, with a smaller contribution from the diffusion-controlled process. However, following the solution tau binding to tau-Au, the impedance dramatically decreased (b) as shown in Fig. 2B. At this point, tau-tau-Au surface was formed. Moreover, the tau binding to the surface dramatically decreased the charge transfer resistance to 0.36 ± 0.08 kΩ. The R_{ct} of tau-tau-Au was reduced to about 1/10 of tau-Au as a result of solution tau binding to immobilized tau on the surface. The tau binding to tau-Au produced the 90 ± 3 % decrease in R_{ct}. The electron transfer from redox probe to Au electrode was largely diffusion-controlled for tau-tau-Au (b) in stark contrast to tau-Au (a). The electrochemical parameters of tau-tau-Au, derived by fitting the experimental data to a circuit (Fig. 2B inset), are presented in Table 1. The decrease in the diameter of the semi-circle upon formation of tau-tau-Au may indicate the development of positive charge on the surface or conformational change of protein film, or both.

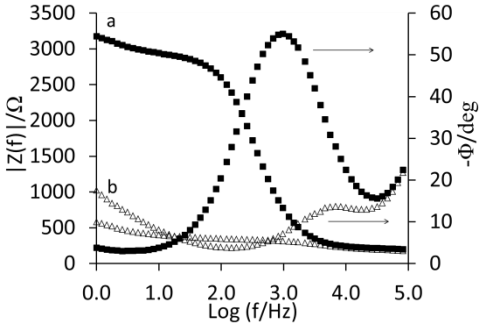

Fig. 3 Bode plots of tau-Au (a) and tau-tau-Au (b) (tau-Au (squares), tau-tau-Au (triangles), 10 mM phosphate buffer pH 6.8, 10 mM $[Fe(CN)_6]^{3-/4-}$).

The Q increased from 0.58 ± 0.33 for tau-Au to 16.4 ± 7.31 $\mu\Omega^{-1}\cdot s^n$ for tau-tau-Au. The large difference in Q components of these two films may indicate a large difference in permeability of redox probe, binding of tau protein onto tau-Au, change in electrostatic protein map and/or conformation of protein film.

Since tau-Au did not undergo change in impedance or *CPE* as a function of measurements in the absence of tau binding, we may conclude that the decrease in impedance and the increase in *CPE* were due to tau binding to tau-Au interface. The large deviation of the exponential factor, n, for tau-tau-Au (0.39 ± 0.07) compared to tau-Au (0.89 ± 0.01) indicates a deviation from ideal capacitive behaviour. This deviation represents a non-smooth surface pointing to the dramatic change in protein film after tau binding. The interaction of solution tau with tau-Au interface influenced the impedance at frequencies below 3000 Hz as depicted in Fig. 3. At higher frequencies, the responses for tau-Au (a) and tau-tau-Au (b) were predominantly controlled by solution resistance. The tau binding to tau-Au surface dramatically modified the impedance amplitude at low frequencies. In Bode plot the impedance between 1 – 130 Hz was five times lower for tau-tau-Au than tau-Au. The Bode plots of tau-Au (a) and tau-tau-Au (b) in Fig. 3 represent only one time constant feature which indicates that tau-Au and tau-tau-Au behave like single layers. In addition, the phase angle dramatically decreased from 55 ° (tau-Au) to 13 ° (tau-tau-Au). Notably, the peak frequency of the phase angle increased from 825 Hz (tau-Au) to 5620 Hz (tau-tau-Au). Therefore the protein-biosensor operates in the low frequency range which was useful for tau binding detection. The high frequency range was not useful for detection of tau-tau binding.

To address the contribution of the ionizable tau film on interactions with redox probe, an anionic probe was replaced by a cationic probe $[Ru(NH_3)_6]^{2+/3+}$.[34-36] The tau-Au was measured in the presence of $[Ru(NH_3)_6]^{2+/3+}$ before and after tau binding. CV profiles of tau-Au and tau-tau-Au were similar (Fig. S12, ESI†). EIS of tau-tau-Au in the presence of $[Ru(NH_3)_6]^{2+/3+}$ resulted in a larger semi-circle component due to increased repulsion between the positively charged surface and the positively charged probe. Upon electrostatic change in tau-tau-Au, the $[Ru(NH_3)_6]^{2+/3+}$ probe was repelled, producing an increase in R_{ct}, while negatively charged probe $[Fe(CN)_6]^{3-/4-}$ was attracted, producing a dramatic

decrease in the R_{ct}. The $[Fe(CN)_6]^{3-/4-}$ and $[Ru(NH_3)_6]^{2+/3+}$ operate under different mechanisms. The $[Ru(NH_3)_6]^{2+/3+}$ can penetrate into layers and diffuse along the layer chains, independent of the probable collapse sites, unlike $[Fe(CN)_6]^{3-/4-}$. In addition, $[Ru(NH_3)_6]^{2+/3+}$ underwent outer-sphere electron transfer, while $[Fe(CN)_6]^{3-/4-}$ probe underwent inner-sphere electron transfer.[37] The outer sphere electron transfer mechanism of $[Ru(NH_3)_6]^{2+/3+}$ probe may involve the approach of redox species to the modified electrode surface and electron exchange with the metal at minimal distances. By contrast, if the mechanism is inner-sphere than very thin, compact monolayer may prevent the direct access of the Au electrode surface to the redox probe and reduce electron transfer rates. The electrochemical data with the positively and negatively charged probes indicated the increase in positive charge upon tau-tau-Au surface formation.

Usually the high peak current in CV corresponds to the low impedance value when $[Fe(CN)_6]^{3-/4-}$ redox probe is used.[14] The decreased current and increased peak potential separation observed in CV are typically followed by the increase in electron transfer resistance.[38-39] This was in stark contrast to the electrochemical data for tau-Au and tau-tau-Au. The tau-tau-Au exhibited lower peak current than tau-Au, but dramatically lower impedance which may suggest the electrostatic and conformational changes upon solution tau binding to tau-Au surface. Other reports exist on a decrease of R_{ct} upon protein binding to the surface layer. For example, when a largely negatively charged aptamer was attached to an electrode, a redox probe exhibited large charge transfer resistance.[40,41] However, the binding of a positively charged protein to aptamer *via* electrostatic interactions introduced a positive charge to which the probe was attracted. In turn, this attraction produced the decrease in R_{ct} despite the protein-aptamer binding on surface. The R_{ct} in EIS measured the resistance to the redox probe, and was sensitive to the electrostatic charge within the protein layer which promoted the electron transfer rate. The high current in CV was followed by the high resistance in EIS when diaminonaphthalene film was immobilized on carbon nanotube electrode.[42] This trend was ascribed to poor conductivity of film and lower diffusivity of ions due to the negative charge of $[Fe(CN)_6]^{3-/4-}$ which adsorbed onto the film.[42] However, the interpretation of the change in R_{ct} is challenging because it may be due to a diffusion of ions through the film, increased positive charge through the film, or conformational change of protein film, among other factors.[43] At pH 6.8, tau is overall positively charged. Under given experimental conditions, when tau binds tau-Au surface, the local ion concentration will increase leading to enhanced electrostatic interactions with the negatively charged redox probe, decreased R_{ct}, and increased *CPE*. The conformational change may also modulate R_{ct}. The reduction in R_{ct} was observed upon fibronectin binding to the polystyrene/thiol/Au surface.[44] For neutravidin, Fab fragment and antibody binding to IgG/Au electrode, the decreased R_{ct} and *CPE* were attributed to change in structure of mixed modified electrode, and inhomogeneity of the layers.[45] Similarly, tau binding to tau-Au may produce electrostatic and conformational changes and decrease in R_{ct}.

The possibility of the tau *N*-tail and *C*-tail folding over its middle domain, termed the "paper-clip" has been previously suggested.[46] The electrostatic interactions between *N*- and *C*-termini hold this conformation in place. Other reports indicated that the extended S-shaped conformation is likely, where termini are away from each other but folding over the middle domain.[37] Tau protein contains R domains (middle domain) which are thought to be involved in tau-tau interactions. In turn, the tau-tau binding *via* R repeat domains of solution tau and immobilized tau may not take place due to the interferences from the *N*- and *C*-termini. Hence, if tau-Au had a "paper clip" or S-conformation to which solution tau (in similar conformation) must bind *via* R domains, then the interactions between *N*-terminal and/or *C*-terminal with the middle domain must be broken. In turn, solution tau binding to immobilized tau induces dramatic conformational change, involving either of two termini and new electrostatic interactions. We propose that a tau-tau-Au film has dramatically different electrochemical properties from tau-Au as a result of conformational and electrostatic changes induced by tau-tau binding.

3.3 Optimization of experimental conditions

To quantify the electrochemical change upon solution tau binding to tau-Au interface, the percent change of R_{ct}, represented by $\Delta R_{ct,}$ was calculated by dividing the change in R_{ct} ($R_{ct(tau\text{-}tau\text{-}Au)}$-$R_{ct(tau\text{-}Au)}$) by the $R_{ct(tau\text{-}Au)}$ as described in the eqn (4) below:

$$\Delta R_{ct} = (R_{ct(tau\text{-}tau\text{-}Au)}\text{-}R_{ct(tau\text{-}Au)})/R_{ct(tau\text{-}Au)}) \times 100\% \quad (4)$$

Hence, the negative and positive values of ΔR_{ct} denoted the decrease and increase in R_{ct} during binding studies, respectively. The solution tau binding to tau-Au occurred fast (within 1 min) at 37 °C and produced -85 ± 5 % ΔR_{ct} (Fig. S1, ESI†). With increasing adsorption time, beyond 2 h, little additional decrease in R_{ct} was observed. The current methodologies can detect tau oligomerization or aggregation only after 10 minutes, which makes this electrochemical assay a relatively fast method of detection.[31] The ΔR_{ct} values were slightly lower when binding studies were carried out at 5 °C (-76 ± 4 % ΔR_{ct}) compared to 37 °C (-90 ± 3 % ΔR_{ct}) indicating the interactions involved in binding were somewhat affected by temperature (Fig. S11, ESI†). This is in contrast to the previous reports of dramatically faster tau aggregation into filaments at temperatures above 20 °C.[31] The lack of significant temperature effect on the electrochemical trend may be due to the experimental conditions. The tau-tau binding in the early steps of tau oligomerization, which was monitored here, may be unaffected by temperature, compared to fibrilization at the later stage. The increase in the ionic strength of the buffer up to 500 mM during binding induced the 95 ± 0.5 % decrease in R_{ct} indicating that the interactions involved in tau-tau binding are unlikely due to salt bridges. Similar findings were reported for the insoluble tau filaments of tau which were largely resistant against the changes in ionic strength.[46]

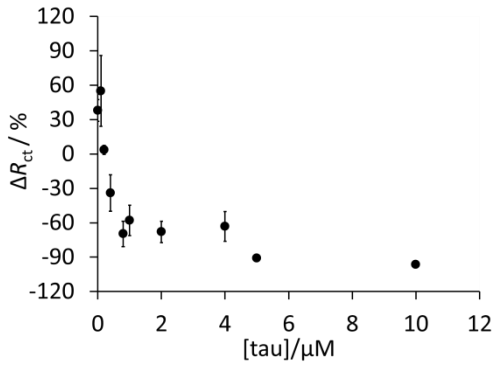

Fig. 4 The plot of the percent change in R_{ct} (ΔR_{ct}) as a function of solution tau concentration during binding to tau-Au surface.

The solution tau concentration dramatically influenced the binding. The saturation in ΔR_{ct} was observed at the solution tau concentration of 1 μM. The plot of ΔR_{ct} as a function of solution tau concentration is presented in Fig. 4. The linear dependence of the ΔR_{ct} *versus* solution tau concentration was observed in the 0.1 – 1.0 μM range. The ΔR_{ct} decreased with the increase in solution tau concentration. The reported micromolar tau concentration was required for aggregation *in vivo*. Here, the tau-tau binding was observed at tau concentration as low as 0.2 μM which makes this electrochemical assay at least 5 times more sensitive than the current optical and microscopic methods.[31]

By changing the pH of tau solution during binding studies, the net charge of the tau protein may be varied. The isoelectric point (*pI*) of tau protein is 8.6, and at pH 6.8 tau is overall positively charged adopting a "paper-clip" or S-shaped conformation.[46] When the binding studies were performed at pH to 8.5, the tau protein was overall zero charged. Since the *pIs* of *N*- and *C*-termini regions of tau are 3.8 and 10.8, respectively, changing the incubation pH from 6.8 to 8.5 was not expected to have an impact on its "paper-clip" or S-conformation. The ΔR_{ct} for tau-tau-Au after incubation at pH 8.5 (-69 ± 5 %) was lower than that at pH 6.8 (-90 ± 3 %) (Fig. S4, S10, ESI†). This decrease in ΔR_{ct} was an indication of the lower binding affinity between solution tau and tau-Au surface when tau protein was overall neutral. However, the smaller ΔR_{ct} value at higher pH may also be due to the electrostatic change on the surface. Recently, it has been suggested that at pH ~6 the histidine residues of tau are involved in its aggregation.[31] The histidine residues in the R regions may be important in solution tau binding to immobilized tau, and in addition to other residues may explain the greater impedance change at pH 6.8. Reports on the aggregation of tau fragments indicated lack of self-association at pH 8.5, while in this study tau binding was observed. While we cannot infer the secondary tau structure from our measurements, these conformational and electrostatic changes leading to impedance decrease may indicate propensity for secondary structure upon tau-tau binding. The loss of long range interactions between *N-/C*-termini and R domains during conformational change was recently ascribed to onset of aggregation.[47] The two tau molecules may be held together by complementary interactions of the *N*-terminal and the central region of each tau molecule, as was predicted for tau binding to microtubules.[48] Hence the formation of tau-tau-Au may result in the conformational and/or electrostatic changes of tau film which facilitate approach of the redox probe toward the electrode where charge transfer is efficient. Also, the increase in the positive charge of tau film may increase the affinity of $[Fe(CN)_6]^{3-/4-}$ probe. The solution tau binding to tau-Au may have created partial interfacial openings or channels to faradaic activity. Since the R_{ct} measures the redox probe mobility and diffusive access to the Au electrode, the generation of interfacial gates may have improved this process *via* conformational or electrostatic change in tau film.[49]

3.4 Surface characterization of tau-Au and tau-tau-Au

To gain information about other aspects of tau film during binding, such as film thickness and wettability, the ellipsometry and contact angle measurements were carried out. Ellipsometry was used to measure the average thickness of tau-Au and tau-tau-Au. Each data set was compared to the bare Au electrode and normalized. For estimation of the film thickness, the refractive index of protein film, n_{film}, and extinction coefficient, k_{film}, were assumed to be 1.5 and 0, respectively.[50,51] Similar film thicknesses (~8 nm) for tau-Au and tau-tau-Au were observed pointing to a lack of film collapse, lack of film decomposition, and negligible thickness change after solution tau binding to tau-Au. This was in agreement with our electrochemical data indicating rearrangement of tau film, increased permeability, and conformational change upon tau binding to tau-Au.

To address the wettability of the tau surface the contact angle was measured. Typically, a relatively hydrophobic surface would exhibit large contact angle to aqueous solution.[52] Under the experimental conditions, the phosphate buffer contact angle of bare Au was at 72 ± 9 °. The contact angle of tau-Au was 47 ± 4 ° due to the presence of more hydrophilic groups. After tau binding to tau-Au, a slight decrease in contact angle to 40 ± 2 ° suggested increased polarity of the surface layers. The rearrangement of tau film upon tau binding may cause the change in orientation of protein domains producing a more hydrophilic surface with greater positive charge. This was in accord with the electrochemical data which suggested that the increased positive charge produced increased permeability to the redox probe and conformational change, following the tau-tau-Au formation.

3.5 Selectivity of tau-Au biosensor

To demonstrate the utility of the tau-based biosensor for detection of tau-tau binding, the electrochemical format has to demonstrate selective response against other proteins. To address selectivity of tau-Au surface, the binding studies were performed with various solutions as shown in Fig. 5. The tau-tau-Au surface was included as a reference. In the absence of solution tau during binding studies (buffer-tau-Au), the ΔR_{ct} increased only 38 ± 9 % presumably due to dynamic changes of tau-Au film (Fig. S6, ESI†). To address the non-specific tau binding, the Au electrode was prepared without immobilized tau, but it contained the lipoic acid *N*-hydroxysuccinimide ester, ethanolamine and hexanethiol components.

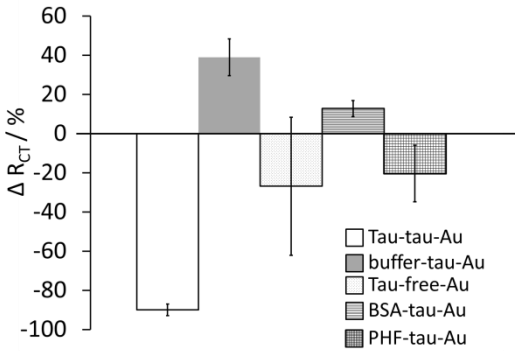

Fig. 5 The plot of the percent change in R_{ct} (ΔR_{ct}) of tau-tau-Au, buffer-tau-Au, tau-free-Au, BSA-tau-Au and PHF-tau-Au (buffer-tau-Au surface lacked solution tau and tau-free-Au surface lacked immobilized tau protein).

The binding of solution tau to the tau-free-Au surface resulted in -26 ± 35 % ΔR_{ct} (Fig. S8, ESI†). The drop in impedance was ascribed to the nonspecific interactions between solution tau and the surface. To address the selectivity of tau-Au interface, the binding studies were carried out with bovine serum albumin (BSA) instead of tau (BSA-tau-Au). The ΔR_{ct} increased only 12 ± 4 % suggesting a minimal non-specific interaction between tau-Au and BSA in solution, and a minimal BSA adsorption and binding (Fig. S7, ESI†). Hence, a highly specific and selective binding of tau to tau-Au surface produced a decrease in R_{ct}. The ΔR_{ct} decreased only 18 ± 10 % in the presence of paired helical filaments (PHF) (Fig. 5). The PHF sample contained a mixture of various tau isoforms, and phosphorylated and truncated tau proteins.[53] Notably, the tau-Au interface was insensitive to PHF (Fig. S13, ESI†) but highly sensitive to nonphosphorylated monomeric tau protein.

The combined electrochemical and surface data demonstrated that the tau-Au was a stable biosensing interface and did not collapse or decompose, pointing to the durability of the protein film. Tau-tau binding on the surface induced conformational and/or electrostatic changes which modulated the charge transfer resistance of the system. Upon tau-tau-Au formation, the film thickness remained unchanged but polarity of the protein surface was slightly affected further supporting the electrochemical trend. The binding of solution tau to tau-Au surface induced conformational and/or electrostatic change pointing to the importance of early tau-tau interactions in the tau aggregation pathway.

4. Conclusions

In summary, the electrochemical detection of tau-tau binding was demonstrated toward development of a new methodology for detection of tau misfolding. The tau-tau binding was monitored by electrochemical impedance spectroscopy *via* modulation in the charge transfer resistance and as a function of concentration of solution tau. The lower impedance and higher capacitance were ascribed to the increased positive charge within the film and conformational change of protein due to tau-tau binding. The study provides qualitative and quantitative data on the tau-tau interactions involved in the early self-assembly of tau protein. The mechanism of tau-tau interaction which drive tau binding to the surface is still unclear and requires further investigation. We predict that such strategy will find applications in determining the key events in early stages of tau protein misfolding and aggregation. Ultimately, this electrochemical approach may be used for monitoring protein conformational change and folding in complex systems, for other proteins than the tau protein. The utility of the electrochemical assay may be extended to inhibitor screening aimed at tau misfolding in search of neurodegenerative therapeutic targets.

Acknowledgments

The authors thank the Department of Chemistry and Oakland University for financial support. SM thanks Oakland University-Beaumont Multidisciplinary Research Grant for funding. HT thanks the Elizabeth A. Kenny Merit Scholarship for the support.

Notes and references

Department of Chemistry, Oakland University, 2200 North Squirrel Road, Rochester, MI, USA, 48309. Fax: 1-248-3702321; Tel: 1-248-3703088; E-mail: martic@oakland.edu

† Electronic Supplementary Information (ESI) available: cyclic voltammograms, electrochemical impedance spectroscopy, desorption data, contact angle and ellipsometry measurements. See DOI: 10.1039/b000000x/

1 I. Grundke-Iqbal, K. Iqbal, Y. C. Tung, M. Quinlan, H. M. Wisniewski and L. I. Binder, *Proc. Natl. Acad. Sci. U. S. A.*, 1986, **83**, 4913-4917.
2 J. Lewis, E. McGowan, J. Rockwood, H. Melrose, P. Nacaraju, M. van Slegtenhorst, K. Gwinn-Hardy, M. Paul Murphy, M. Baker, X. Yu, K. Duff, J. Hardy, A. Corral, W. L. Lin, S. H. Yen, D. W. Dickson, P. Davies and M. Hutton, *Nat. Genet.*, 2000, **25**, 402–405.
3 V. M. Lee, B. J. Balin, L. Jr. Otvos and J.Q. Trojanowski, *Science*, 1991, **251**, 675–678.
4 K.S. Kosik, C. L. Joachim and D. J. Selkoe, *Proc. Natl. Acad. Sci. U. S. A.*, 1986, **83**, 4044-4048.
5 S. Elbaum-Garfinkle and E. Rhoades, *J. Am. Chem. Soc.*, 2012, **134**, 16607-16613.
6 P. Friedhoff, A. Schneider, E. M. Mandelkow and E. Mandelkow, *Biochemistry*, 1998, **37**, 10223-10230.
7 M. Kidd, *Nature*, 1963, **197**, 192-193.
8 C. A. Lasagna-Reeves, D. L. Castillo-Carranza, U. Sengupta, A. L. Clos, G. R. Jackson and R. Kayed, *Mol. Neurodegener.*, 2011, **6**, 39-53.
9 P. V. Arrigada, J. H. Growdon, E. T. Hedley-Whyte and B. T. Hyman, *Neurology*, 1992, **42**, 631–639.
10 M. von Bergen, P. Friedhoff, J. Biernat, J. Heberle, E. M. Mandelkow and E. Mandelkow, *Proc. Natl. Acad. Sci. U. S. A.*, 2000, **97**, 5129-5134.
11 C. A. Rankin, Q. Sun and T. C. Gamblin, *Mol. Neurodegener.*, 2007, **2**, 12-26.
12 D. W. Cleveland, S. Y. Hwo and M. W. Kirschner, *J. Mol. Biol.* 1977, **116**, 227-247.
13 S. Barghorn and E. Mandelkow, *Biochemistry*, 2002, **41**, 14885-14896.
14 A. J. Bard and L. R. Faulkner, *Electrochemical Methods Fundamentals and Applications*, Wiley, New York, 1980.
15 E. Katz and I. Willner, *Electroanalysis*, 2003, **15**, 913-947.
16 R. K. R. Philips, S. Omanovic and S. G. Roscoe, *Langmuir*, 2001, **17**, 2471-2477.
17 S. G. Roscoe, K. L. Fuller and G. Robitalle, *J. Colloid Interface Sci.* 1992, **152**, 429-441.
18 J. D. Tirado, D. Acevedo, R. L. Bretz and H. D. Abruna, *Langmuir*, 1994, **10**, 1971-1979.

19 V. Ostatna, H. Cernocka and E. Palecek, *Bioelectrochemistry*, 2012, **87**, 84-88.
20 M. Bartosik, V. Ostatna and E. Palecek, *Bioelectrochemistry*, 2009, **76**, 70-75.
21 L. Chen-Zhong, Y.T. Long, J. S. Lee and H.-B. Kraatz, *Chem. Commun.* 2004, 574-575.
22 A. Bogomolova, E. Komarova, K. Reber, T. Gerasimov, O. Yavuz, S. Bhatt and M. Aldissi, *Anal. Chem.* 2009, **81**, 3944-3949.
23 A. C. Barton, F. Davis and S. P. Higson, *Anal. Chem.* 2008, **80**, 9411-9416.
24 G. Tsekenis, G. Z. Garifallou, F. Davis, P. A. Millner, T. D. Gibson and S. P. Higson, *Anal. Chem.* 2008, **80**, 2058-2062.
25 M. K. Rains, S. Martic, D. Freeman and H.-B. Kraatz, *ACS Chem. Neurosci.*, 2013, **4**, 1194-1203.
26 S. Martic, S. Beheshti, M. K. Rains and H. B. Kraatz, *Analyst*, 2012, **137**, 2042-2046.
27 A. Boutajangout, J. Ingadottir, P. Davis and E. M. Sigurdsson, *J. Neurochem.*, 2011, **118**, 658-667.
28 A. Gruzman, A. Hidmi, J. Katzhendler, A. Haj-Yehie, S. Sasson, *Bioorg. Med. Chem.*, 2004, **12**, 1183-1190.
29 A. S. Bandarenka, *Analyst*, 2013, **138**, 5540-5554.
30 M. Manesse, V. Stambouli, R. Boukherroub and S. Szunerits, *Analyst*, 2008, **133**, 1097-1103.
31 P. Fridhoff, A. Schneider, E. M. Mandelkow and E. Mandelkow, *Biochemistry*, 1998, **37**, 10223-10230.
32 C. Liu, S. Dong, G. Cheng and D. Y. Sun, *J. Electrochem. Soc.*, 1996, **143**, 3874-3880.
33 D. J. Chung, S. H. Oh, S. Komathi, A. I. Gopalan, K. P. Lee and S. H. Choi, *Electrochim. Acta*, 2012, **76**, 394-403.
34 J. Ghilane, G. Trippe-Allard and J. C. Lacroix, *Electrochem. Commun.* 2013, **27**, 73-76.
35 R. G. Nuzzo, L. H. Dubois and D. L. Allara, *J. Am. Chem. Soc.* 1990, **112**, 558-569.
36 M. Steichen, Y. Decrem, E. Godfroid and C. Buess-Herman, *Biosens. Bioelectron.* 2007, **22**, 2237-2243.
37 M. Fleischmann, P. R. Graves and J. Robinson, *J. Electroanal. Chem.* 1985, **182**, 87-98.
38 H. Qi. C. Ling, R. Huang, X. Qiu, L. Shangguan, Q. Gao and C. Zhang, *Electrochim. Acta*, 2012, **63**, 76-82.
39 F. T. C. Moreira, R. A. F. Dutra, J. P. C. Noronha and M. G. F. Sales, *Electrochim. Acta*, 2013, **107**, 481-487.
40 A. Johnson, Q. Song, P. K. Ferrigno, P. R. Bueno and J. J. Davis, *Anal. Chem.*, 2012, **84**, 6553-6560.
41 M.C. Rodriguez, A-N. Kawde and J. Wang, *Chem. Commun.*, 2005 4267-4269.
42 J. Zhang, S. Yang, H. Wang and S. Wang, *Electrochim. Acta*, 2012, **15**, 467-474.
43 M. Luo, A. Amegashie, A. Chua, G. K. Olivier and J. Frechette, *J. Phys. Chem. C* , 2012, **116**, 13964-13971.
44 A. Bouafsoun, S. Helali, S. Mebarek, C. Zeiller, A. F. Progent, A. Othmane, A. Kerkeni, N. Jaffrezic-Renault and L. Ponsonnet, *Bioelectrochemistry*, 2007, **70,** 401-407.
45 S. Hleli, C. Martlet, A. Abdelghani, N. Burais and N. Jaffrezic-Renault, *Sensors and Actuators B*, 2006, **113**, 711-717.
46 S. Jeganathan, M. von Bergen, E. V. Mandelkow and E. Mandelkow, *Biochemistry*, 2008, **47**, 10526-10539.
47 S. Elbaum-Garfinkle and E. Rhoades, *J. Am. Chem. Soc.* 2012, **134**, 16607-16613.
48 K. J. Rosenberg, J. L. Ross, H. E. Feinstein, S. C. Feinstein and J. Isrealachvili, *Proc. Nat. Acad. Sci. U. S. A.* 2008, **105**, 7445-7450.
49 P. Harder, M. Grunze and R. Dahint, *J. Phys. Chem.* 1998, **102**, 426-436.
50 V. Reipa, A. K. Gaigalas and V. L. Vilker, *Langmuir*, 1997, **13**, 3508-3514.
51 K. Rechendorff, M. B. Hovgaard, M. Foss, V. P. Zhdanov and F. Besenbacher, *Langmuir*, 2006, **22**, 10885-10888.
52 T. Onda, S. Shinuichi, N. Satoh and K. Tsujii, *Langmuir*, 1996, **12**, 2125-2127.
53 S. G. Greenberg, P. Davis, J. D. Schein and L. I. Binder, *J. Biol. Chem.*, 1992, **267**, 564-569.

Table of content graphic:

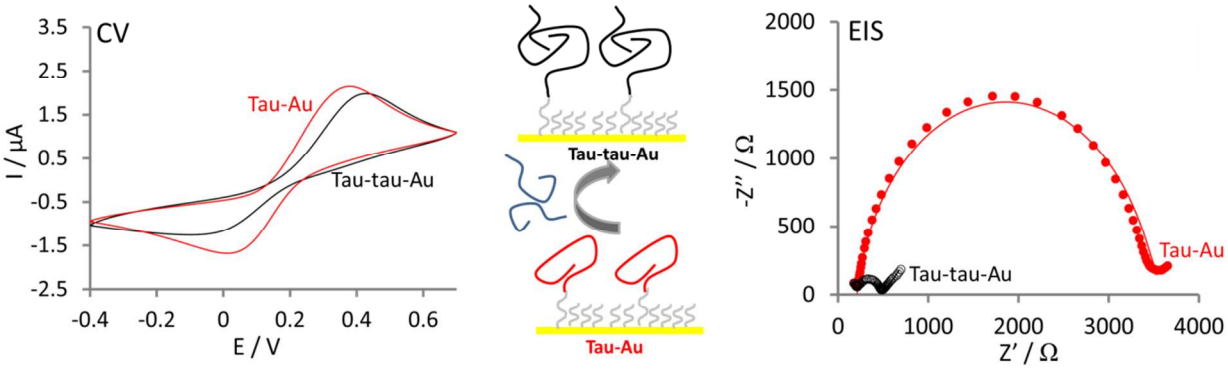

Tau-tau binding induced the electrostatic and conformational change on surface modulating the charge transfer resistance.